Quenching and Partitioning of Plate Steels: Partitioning Design Methodology

R.A. STEWART, J.G. SPEER, B.G. THOMAS, E. DE MOOR, and A.J. CLARKE

Quenching and partitioning (Q&P), a new heat treatment concept to develop high-strength martensitic microstructures with retained austenite (RA), has been implemented industrially to make sheet products. This process is also of interest for thicker plate products, to employ transformation-induced plasticity to enhance toughness and/or wear resistance. The applicability of the Q&P process to plate steel is explored considering through-thickness thermal profiles and associated microstructural gradients. Design methodologies are developed for both the quenching and the partitioning steps of plate processing, coupling thermal models with microstructural design concepts. The design methodologies are experimentally validated using a 0.4 wt pct C 300 M alloy through dilatometry simulations of plate Q&P processing, according to numerically simulated profiles. Q&P microstructures were successfully obtained through the thickness of a simulated 18-mm plate, and attractive RA fractions were achieved.

https://doi.org/10.1007/s11661-019-05337-3

I. INTRODUCTION

QUENCHING and partitioning (Q&P)[1] is a heat treatment most frequently applied to low-alloy cold-rolled sheet steels, to develop high-strength martensitic microstructures with retained austenite (RA).[2] The austenite is stabilized by partitioning of carbon from supersaturated martensite. Such microstructures provide excellent combinations of strength, ductility, and formability, which are of interest to the automotive industry.[3] Q&P is also of interest for thicker plate products, to employ transformation-induced plasticity (TRIP) in microstructures containing austenite to enhance toughness and/or wear resistance for applications such as ground-engaging machinery.[4,5] Toughness of these steels is known to increase with the amount of retained austenite, due to volume expansion during TRIP, causing blunting of crack tips.[4–8]

A schematic illustration of a generic Q&P process is shown in Figure 1. The process involves an initial quenching step following austenitization to a carefully controlled quench temperature (QT) where a desired fraction of martensite is formed. The QT is often selected according to a methodology which predicts an "optimum" QT where the most austenite could be retained, based on "ideal" partitioning.[9,10] The controlled mixture of martensite and austenite formed during the quenching step undergoes partitioning during holding at a partitioning temperature (PT) for a partitioning time (Pt). During the partitioning step, a substantial portion of the carbon in the martensite diffuses into the austenite, thereby stabilizing it. Final cooling to room temperature completes the process and may result in formation of "fresh" martensite. The QT selection methodology is used widely in the Q&P sheet literature,[11–16] although measured RA fractions are typically less than final predicted RA fractions calculated based on the basic constrained carbon equilibrium model; final RA fractions have been shown to be less sensitive to the QT than expected, in both experimental and modeling studies of a 0.19C-1.59Mn-1.63Si (wt pct) over a range of 60 °C,[15] when considering partitioning kinetics.

Q&P steels are also industrially produced as a hot-rolled sheet product,[19] where partitioning takes place during coil cooling. The process does not follow the schematic shown in Figure 1; slow coil cooling and partitioning begin at the end of the quench step and there is typically no subsequent reheating. The use of coil cooling as a partitioning step was first proposed by Thomas *et al.*,[20] who also suggested a method to estimate the "degree" of partitioning.

A variety of other Q&P process variations have been studied,[21–23] but only a small number of studies have examined the applicability of Q&P processing to thicker sections.[7,24,25] Hong *et al.* were the first to produce Q&P plate under laboratory conditions. A subsequent study by Somani *et al.*[26] showed properties of laboratory hot-rolled direct quenched and partitioned plate at a thickness of 11.2 mm comparable to laboratory

R.A. STEWART, J.G. SPEER, B.G. THOMAS, E. DE MOOR, and A.J. CLARKE are with the Colorado School of Mines, Golden, CO. Contact e-mail: rachaelstewart@alumni.mines.edu
Manuscript submitted December 23, 2018.
Article published online August 5, 2019

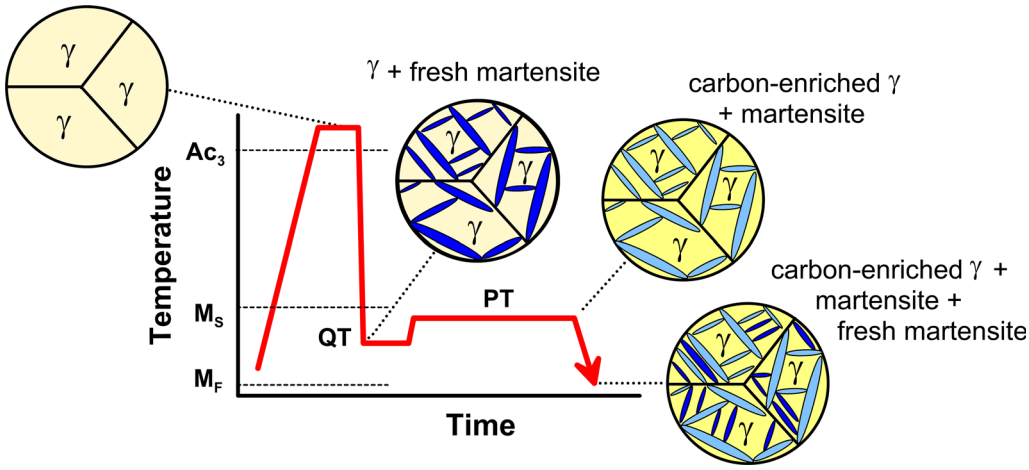

Fig. 1—Schematic of 2-step Q&P sheet thermal processing, with full austenitization. QT and PT are quenching and partitioning temperatures, respectively. Ms and Mf are the martensite start and finish temperatures. Expected microstructures at each step are illustrated Ref. [7].

produced sheet Q&P steels: ultimate tensile strength levels of laboratory rolled plate[26] were similar to levels achieved in laboratory processed sheet[27] and comparable amounts of austenite were retained in the two product forms.[26–28] However, in the hot-rolled plate, inhomogeneous microstructures were noted through the plate thickness.[26] Similarly, in a study by Zhou *et al.*,[24] a quench-partition-temper process produced inhomogeneous microstructures in a 20-mm-thick laboratory processed steel: lath martensite formed at the surface and subsurface, while a multi-phase microstructure of lath martensite and bainite was observed in the core. The difference in cooling rates from the surface to the inner region of the sample resulted in microstructural variation, as the core temperature remained above the M_s temperature for a longer period of time than the surface regions. These findings highlight the challenges associated with Q&P processing of thicker sections. Variation in cooling rate through the thickness produces thermal gradients and potentially results in non-uniform microstructures through the thickness.

A previous study by the authors focused on understanding the thermal histories developed in plates with varying thicknesses (6 to 50 mm) under three quench media (air cooling, spray water cooling, and severe water quenching) using thermal modeling.[29] The thermal histories obtained from numerical modeling were used to predict the phase fractions at every location through thickness during quenching. Applying the methodology used in earlier Q&P studies based on "ideal" partitioning,[10] the final phase fractions were also predicted. These predictions were used to develop a design methodology for the quench step. The initial phase fractions vary with the quenching time, which can be selected such that the "optimum" QT is achieved at a desired location in the plate cross section.

Results obtained using this methodology are illustrated in Figure 2. Using numerically simulated profiles presented in a previous study,[29] the Koistinen–Marburger equation was applied to the thermal history of a severe water quenched 18-mm plate. The cooling rate at the surface of the 18-mm plate, between 800 °C and 500 °C (at the surface), is 273 °C/s under a sever water quench; the center (mid-thickness) cooling rate is 72 °C/s. Predicted phase fractions are shown for a 300 M alloy steel for which the "optimum" QT is 208 °C and corresponds to 41 vol pct retained austenite. Selection of the quarter point for optimization set the quenching time. Under a severe water quench, the quarter point reaches 208 °C at 15.2 seconds. Figure 2 shows the predicted phase fractions for the 18-mm plate at the end of the quench step, and the phase fractions after final quenching assuming "ideal" partitioning. After initial quenching, the plate surface contains 84 vol pct martensite, the quarter point contains 59 vol pct martensite and the plate center contains 40 vol pct RA. After final quenching, the quarter point contains 41 vol pct RA, stabilizing all of the austenite remaining in this location after quenching. Some fresh martensite forms between the plate quarter point and center during final quenching and the remainder of the microstructure is 'partitioned' martensite.

The quenching step is important in controlling the amount of austenite that might be stabilized during partitioning. The actual amount and the stability of the austenite retained after final quenching also depends on the effectiveness of the partitioning step. To study plate partitioning behavior, the focus of new design methods reported in this paper, the model was extended and applied to plate reheating after quenching. A common plate reheating step in industrial plate production is a furnace temper after quenching. In conventional Q&T steels, reheating is performed after quenching to room temperature, while in Q&P steels quenching would be interrupted after a *partial* martensitic transformation. Partitioning behaviors during off-line plate heat treating, involving the transfer of a quenched plate and reheating in a furnace, were therefore modeled. The quenching process was modeled in an earlier stage of this work.[29] Results for nine cooling scenarios are presented as temperature–time plots in Figure 3. The thermal histories at three positions through the

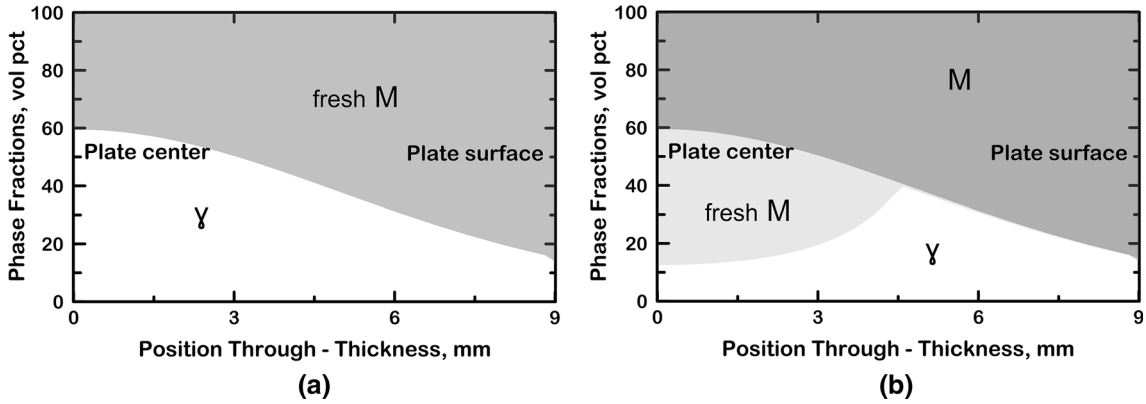

Fig. 2—Estimated (*a*) phase fractions after interrupted quenching and (*b*) final phase fractions at room temperature (assuming full partitioning) for 300 M as a function of position through the plate thickness from center to surface for a quenching time of 15.2 s, wherein the "optimum" quench temperature is reached at the quarter thickness position.

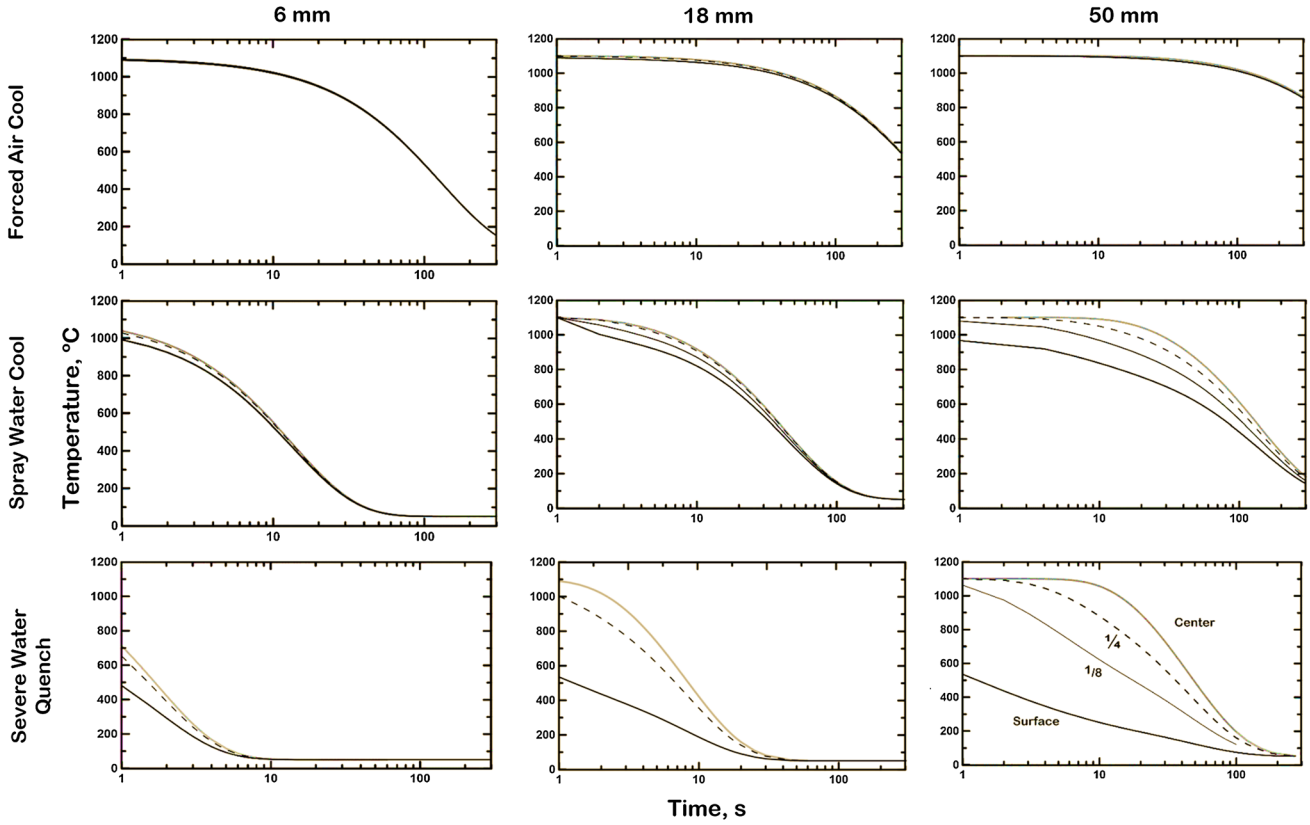

Fig. 3—Thermal histories for plate thicknesses 6, 18, and 50 mm quenched from 1100 °C using three quenching media: severe water quench (convection coefficient, h = 10 000 W/m^2 K), spray water cool (h = 1000 W/m^2 K), and air cool (h = 10 W/m^2 K). Time is shown on log scale from 1 to 300 s. Thermal histories at plate center are indicated with a gray line; quarter thickness position by a dashed line; and surface by a black line.

thickness are shown for the 6-mm and 18-mm plates: center, surface, and quarter point. Four locations are shown for the 50-mm plate: center, surface, quarter point, and eighth point. Thermal histories are shown on a logarithmic scale for quench times between 1 and 300 seconds. Note that the temperature change with respect to distance is referred to as the thermal gradient, and the temperature change with respect to time is referred to as the cooling rate or history. In general, both thermal gradients and cooling rates vary with position through the plate thickness. The chosen quenching case (18 mm severe water quench) represents the starting point of partitioning.

II. ANALYSIS OF HEATING: MODEL FORMULATION AND RESULTS

A one-dimensional computational model was developed to simulate temperature evolution during the cooling and reheating of a flat steel plate.[29]

The thermal model ignores temperature variations near the plate ends and sides due to edge cooling, as the plate thickness is small compared to the length and width. The latent heat of phase transformation was neglected for this study, and constant thermal properties[30,31] and uniform heat transfer to the surface were assumed. Under these assumptions, the transient heat conduction through the flat plate can be described by the one-dimension form of Fourier's transient-conduction equation, given by Eq. [1],

$$\frac{\partial T}{\partial t} = \alpha \frac{\partial^2 T}{\partial x^2}, \qquad [1]$$

where T is the temperature, t is the time, x is the distance through the plate thickness, and α is the thermal diffusivity, defined as

$$\alpha = \frac{k}{\rho C_p}, \qquad [2]$$

where k is the conductivity (W/m K), ρ is the density (kg/m^3), and C_p is the specific heat (J/kg K).

The boundary condition for cooling of the plate surface is based on forced convection with two different constant convection coefficients given in Table I, for severe water quenching, h_q, followed by air cooling during plate transfer, h_t, as discussed in previous work.[29] To simulate furnace reheating of the plate, the surface boundary condition includes two components: forced convection and radiation from the furnace interior as follows.

$$q = h(T_\infty - T_{\text{surf}}) + \varepsilon\sigma\left(T_\infty^4 - T_{\text{surf}}^4\right), \qquad [3]$$

where q is the rate of energy transferred to the plate surface, (W/m^2), ε is the emissivity, h is the convection coefficient (W/m K), σ is the Stefan–Boltzmann constant (5.67×10^{-8} W/m^2 K^4), T_∞ is the ambient temperature (K), and T_{surf} is the current plate surface temperature (K).[32] The view factor with respect to the furnace interior environment was assumed to be unity; that is, 100 pct of the plate surface is exposed to the furnace interior temperature. Boundary conditions were assumed to be identical at the plate top and bottom surfaces which create a symmetry plane at the plate center. The chosen modeled domain is a one-dimensional slice through half the plate thickness (H). An insulated or zero-flux condition was imposed at the plate center (mid-thickness).

The domain was discretized by subdividing it into cells and nodes and developing temperature expressions for each node. Temperature expressions (Eqs. [4], [5] and [6]) were obtained by performing an energy balance on each cell, applying the boundary conditions with neighboring cells, or with ambient temperature when appropriate for surface cells, and expanding Fourier's heat equation. The notation includes a temperature term with indices for position (distance from the plate center), and time, $T^{\text{time}(n)}_{\text{position}(x)}$. The surface cell where the convection and radiation boundary conditions are applied is 'cell n.' The center cell, where the insulated boundary condition is applied, is 'cell 1,' and the other cells comprising the interior are 'cell i.'

$$T_1^{t+1} = T_1^t + \frac{2k\Delta t}{\rho C_p \Delta x^2}\left[T_1^t - T_2^t\right] \qquad [4]$$

$$T_i^{t+1} = T_i^t + \frac{k\Delta t}{\rho C_p \Delta x^2}\left[T_{i+2}^t - 2T_{i+1}^t + T_i^t\right] \qquad [5]$$

$$T_n^{t+1} = T_n^t + \frac{2k\Delta t}{\rho C_p \Delta x^2}\left[T_{n-1}^t - T_n^t\right] + \frac{2h\Delta t}{\rho C_p \Delta x}\left[T_\infty - T_n^t\right] + \frac{2\sigma\varepsilon}{\rho C_p \Delta x}\left[T_\infty^4 - T_n^{t4}\right]. \qquad [6]$$

Table I. Parameters Used in the Thermal Modeling

Parameter	Symbol	Value	Reference
Thermal Conductivity	k	30 W/m K	33
Thermal Diffusivity	α	7.003×10^{-6} m^2/s	33
Specific Heat	C_p	560 J/kg K	33
Density	ρ	7650 kg/m^3	33
Emissivity	ε	0.8	34
Plate Thickness		18 mm	
Initial Temperature	T_{ini}	1100 °C	
Quench Bath Temperature	T_{inf}	50 °C	
Quench Convection Coefficient	h_q	10 000 W/m^2 K	35
Quench Fluid Velocity/Flow Rate		847 L/m^2 s	36
Transfer, Air Cool Convection Coefficient	h_t	10 W/m^2 K	37
Furnace Convection Coefficient	h_f	40 W/m^2 K	37
Quench Time		15.2 s	
Transfer Time		5 min	
Furnace Residence Time		60 min	

A transformed version of Eqs. [4] through [6] was written in Matlab and solved using a built-in Matlab ordinary differential solver (ODE23s) for stiff equations.

The material properties, convection coefficients, and simulation times used in the thermal model are given in Table I. Convection coefficients are given for both the quenching step (quenching) and the partitioning step (transfer and furnace reheating). The schematic thermal history of a quenched plate transferred to a furnace and furnace reheated is shown in Figure 4.

Comparing Figure 4 to the sheet Q&P schematic shown in Figure 1, some important challenges associated with the partitioning step in plate Q&P processing are evident. During quenching, the center, surface, and quarter point of the plate have unique thermal histories, and, at the end of the quench step, each has a unique 'QT.' The 'QT' fixes the martensite fraction (as illustrated in Figure 2). According to previous studies, partitioning begins quickly after quenching[10,11] so that the 'QT' can also be considered to mark the onset of partitioning. Figure 4 shows that, during transfer to the furnace, the plate center and quarter point initially continue cooling, while the plate surface reheats. Within a few seconds of quenching, the plate temperature becomes uniform, and the thermal profiles overlap, as shown in Figure 4. Additional cooling of some locations in the plate after leaving the quench unit could cause additional martensite to form in the interior, so that the phase fractions indicated in Figure 2 may not be applicable everywhere through the thickness. Later in this paper we refer to the "initial QT" and the "final QT" to recognize this complication; the "initial" QT refers to the temperature at a location when quenching is terminated, while the "final QT" represents the lowest temperature expected at that location before heating begins during the partitioning step. It should also be recognized that partitioning may correspondingly be expected to "begin" at different times at different locations through the thickness for portions of the plate that experience "extra" cooling after the quenching step is completed. Besides the complication of a unique partitioning path at each location through the thickness, the partitioning path, which is made up of the transfer step from the quench unit to the furnace and subsequent furnace reheating, is also non-isothermal. The plate cools slowly during transfer, and then during furnace reheating reaches the furnace ambient temperature over a timescale ranging from tens of minutes to an hour, depending on the furnace set temperature. Such long furnace residence times could result in decomposition of austenite, so design of an effective partitioning step according to the thermal history shown in Figure 4 is not obvious. A design methodology was therefore needed to identify transfer and furnace conditions which can be used to achieve effective partitioning under non-isothermal conditions, and account for unique thermal histories through thickness.

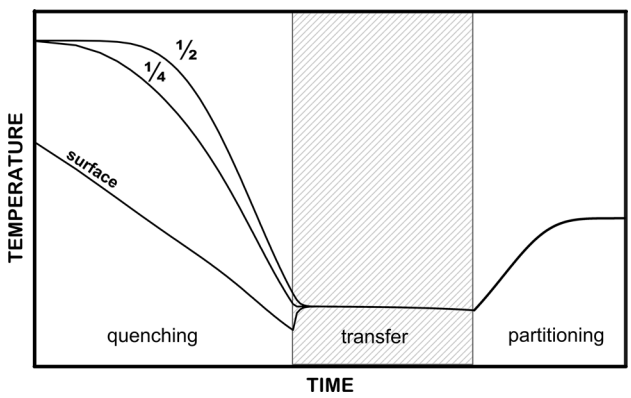

Fig. 4—Schematic of plate Q&P thermal processing, with a quench step, a transfer step from the quench unit to the furnace (indicated with hatched area), and a furnace reheat.

III. PARTITIONING DESIGN METHODOLOGY

Partitioning under non-isothermal conditions was studied earlier by Thomas *et al.*[38] Thomas *et al.* employed the empirically developed Hollomon–Jaffe tempering parameter (TP) to quantify the 'degree of partitioning' for coil-cooled hot strip Q&P. The Hollomon–Jaffe TP relates tempering time and temperature to relative hardness and can be calculated for both isothermal and non-isothermal heat treatments, according to Eqs. [7] and [8], respectively.[39]

$$\mathrm{TP} = T(\log t + c) \qquad [7]$$

$$\mathrm{TP} = T\left(\log \Delta t \times 10^{c} + 10^{TP_o/T}\right), \qquad [8]$$

where t is the time (s), Δt is the duration of a timestep, P_o is the tempering parameter of the beginning of a timestep (zero for the first timestep), T is the temperature (K), and c is a carbon-dependent constant given by Eq. [9].

$$c = 21.3 - 5.8\ (\text{wt pct carbon}). \qquad [9]$$

Estimates based on Eqs. [7] and [8] can be used to identify isothermal and non-isothermal partitioning conditions that are equivalent to one another. Thomas *et al.* used such equivalence to select coiling temperatures for hot-rolled Q&P processing. The TP concept was applied here to the non-isothermal furnace partitioning path for plate steel such as shown in Figure 4, to select transfer times and furnace residence times and furnace temperatures to achieve specified degrees of partitioning. Figure 5 shows non-isothermal TP values calculated along the partitioning path for the quarter point location for a 5-minute transfer and a 60-minute furnace reheat. The partitioning path was assumed to begin at the end of the quench step and, after the plate temperature has reached equilibrium, no substantial thermal gradients are reintroduced so that the calculated TP is essentially identical through the thickness during air cooling and furnace reheating after the first few seconds of quenching. The estimated tempered hardness for a 0.42 wt pct C steel[40] at each TP is indicated on the secondary y-axis. The tempered hardness was

estimated for the examined range of TP from the measured hardness of a 0.42 wt pct C steel after a 1-hour isothermal temper at temperatures between 93 °C and 704 °C (200 °F and 900 °F).[41] Lines of best fit between the calculated isothermal TP and measured hardness over two ranges of tempering temperatures (above and below 426 °C) were used to estimate the hardness for TP between 6000 and 18,000.

For reference, isothermal TPs were also calculated for each of the isothermal hold temperatures indicated in Figure 5 for the time indicated on the *x*-axis. Thus, effective isothermal partitioning treatments, known from the literature, can be translated into non-isothermal treatments in order to select furnace residence times and temperatures.

The TP calculated over the plate partitioning path during the transfer step nearly overlaps the TP for a 200 °C isothermal hold, as the temperature of the plate is about 200 °C after quenching and during subsequent holding in air; the plate enters the furnace at a temperature of 189 °C. During furnace reheating, the non-isothermal TP then increases more rapidly, especially at higher furnace ambient temperatures. Furnace ambient temperatures of 400 °C and 500 °C were considered to provide reasonable furnace residence times for a range of TP. Furnace residence times between 5 and 30 minutes provide a "degree of partitioning" equivalent to TP in the range of 9000 to 12,000 in a 400 °C furnace, and up to TP 13,000 in a 500 °C furnace. A furnace ambient temperature of 600 °C may be attractive for partitioning treatments with TP above 13,000, given the shorter residence times, although alloy design and microstructural evolution must be considered.

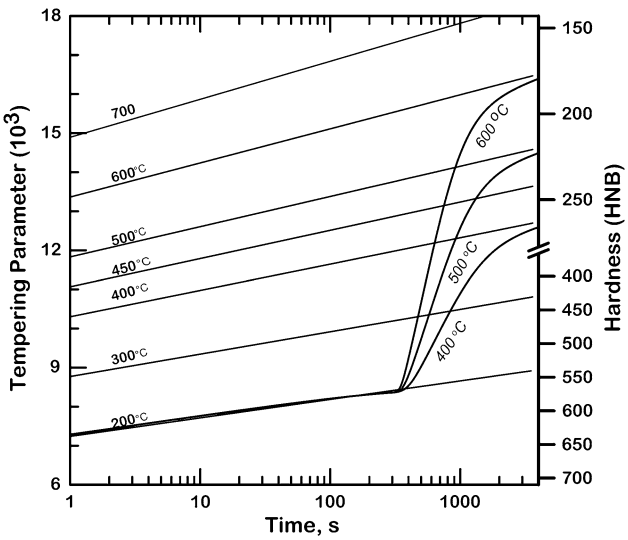

Fig. 5—Non-isothermal tempering parameter evolution with time after quenching an 18-mm plate for 15.2 s, furnace transfer taking 5 min, followed by reheating in a furnace held at 400 °C, 500 °C or 600 °C. Isothermal tempering parameters are also indicated for tempering temperatures between 100 °C and 700 °C. The expected tempered hardness of a 0.42 wt pct C steel is indicated on the secondary *y*-axis in Brinell[38]

To experimentally verify the partitioning design methodology, furnace residence times and furnace temperatures were selected by examining data from the sheet Q&P literature and identifying effective isothermal TP conditions. The effectiveness of a partitioning treatment can be evaluated based on its ability to promote austenite retention at room temperature. To evaluate the correlation between TP and RA, data were collected from a number of Q&P studies.[10,27,42–47] Accordingly, the volume fractions of RA are plotted against the calculated TP in Figure 6 for both 1-step[10,45,47–49] and 2-step[10,27,42–44,46,47] isothermally partitioned Q&P steels. Partitioning treatments in these studies varied and the amount of RA was not necessarily optimized for each treatment. Based on Figure 6, it was concluded that TPs between 8000 and 14,000 provided suitable results in previous studies, so Q&P plate design and experimentation should explore furnace partitioning treatments with TPs within this range.

IV. EXPERIMENTAL METHODS FOR VERIFICATION OF DESIGN METHODOLOGIES

Experimental verification of the quenching and the partitioning design methodologies was conducted through laboratory simulation of Q&P plate processing, according to numerically simulated profiles. Alloy 300 M was selected for experimental exploration, as it

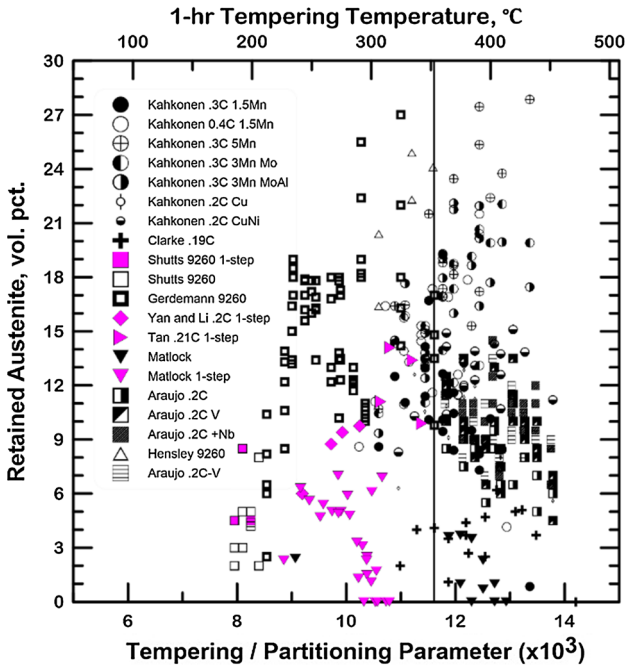

Fig. 6—Retained austenite as a function of tempering/partitioning parameter for Q&P data collected from the literature. All data collected for Q&P heat treatments with full austenitization. One-step partitioning data are indicated with solid gray symbols. The average tempering parameter for all studies is indicated with the vertical line. Equivalent one-hour tempering temperatures for each tempering parameter are indicated using the secondary *x*-axis; actual partitioning treatments varied between 1 s and 3 h.

Table II. Chemical Composition of 300 M, Weight Percent

C	Mn	Si	Ni	Cr	Mo	Ti	Nb	V	Al	S	P	Cu	Sn
0.42	0.72	1.58	1.93	0.8	0.4	0.003	—	0.08	0.038	0.001	0.006	0.12	0.009

contains additions of silicon (needed in Q&P steels to prevent/delay carbide formation[17,27]). 300 M was also selected because of its hardenability; it is expected to be fully hardenable at 18 mm using severe water quenching.[29,50] The material used in the experimental study was commercially produced by electric arc furnace melting, vacuum ladle refining, and bottom pouring into 711 mm (28 in) square ingots. The steel was hot rolled to 215 mm (8.5 in) round-corner bars and received in the as-hot-rolled condition without further heat treatment. The chemical composition of the 300 M material is shown in Table II.

The design methodologies for both the quenching and partitioning steps were applied to alloy 300 M. The quarter thickness location was selected for optimization of the retained austenite amount in the final microstructure, and the predicted evolution of the final microstructure is illustrated for this quenching condition in Figure 2, assuming ideal partitioning.

Based on the developed partitioning design methodology, tempering parameters 8000 10,000 and 12,000 were selected for experimental partitioning treatments, and furnace ambient temperatures of 400 °C and 500 °C were chosen as furnace parameters. Transfer time was fixed at 5 minutes. Furnace residence times for TP 10,000 and 12,000 were obtained from Figure 5. TP 8000 is reached during the transfer step, without additional furnace reheating. The predicted hardness of 300 M was also estimated using Figure 5: 606 Brinell (HNB) for TP 8000, 479 HNB for TP 10,000 and 353 HNB for TP 12,000. It should be noted that the predicted hardness is for a quenched and tempered 0.42 wt pct C steel[51] and may not correspond to the hardness of 300 M after Q&P processing, where carbon is distributed differently through the microstructure in comparison to conventional Q&T.

The process diagram corresponding to the selected processing parameters (and numerical modeling parameters given in Table II) is shown in Figure 7. Time zero refers to the beginning of quenching from 1100 °C, the austenitizing temperature used in the experimental portion of this work. The times at which the desired degrees of partitioning are achieved are indicated in each process diagram with circles. Figure 7 shows the center, surface, and quarter point profiles from the beginning of the quench step to conclusion of the furnace reheating step. The 5-minute austenitization treatment and a final quench to room temperature after furnace reheating are also part of the Q&P process but are not shown in the process diagrams. The furnace residence time is indicated on a second *x*-axis, below the figure.

Two additional quenching conditions were included in the experimental study. Quench times of 13 and 18.2 seconds were selected, corresponding to the time at which the quarter point reaches temperatures 50 °C above and below the "optimum" QT of 208 °C. These conditions were used to assess the sensitivity of the resulting microstructure and hardness to variation in the quenching process. Conventional Q&T conditions with TP 8000, 10,000 and 12,000 were also simulated for reference. The Q&T samples were fully quenched to room temperature and then reheated and isothermally held at 200 °C for 40 seconds, 300 °C for 140 seconds, and 400 °C for 333 seconds for TP 8000, 10,000, and 12,000, respectively.

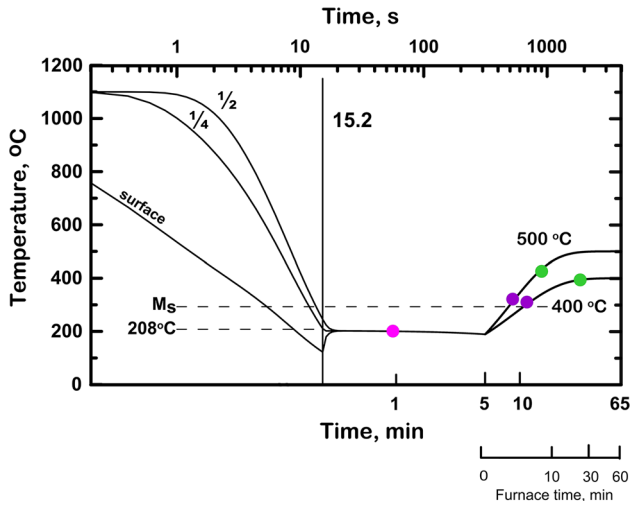

Fig. 7—Q&P process simulated for 18-mm plate severe water quenched for 15.2 s from 1100 °C to 208 °C ("optimum" quench temperature), transferred over 5 min, and reheated in either a 400 °C or 500 °C furnace. Points at which tempering parameters of 8000 10,000 and 12,000 are achieved are indicated by circles. Furnace residence time in minutes (0 to 60 min) is indicated on the additional axis below the figure.

Experimental simulations of the designed Q&P processes were performed using the Thermal Analysis (TA) Quenching Dilatometer DIL805L. Samples were processed to match the thermal profiles at the center, surface, and quarter point of the 18-mm plate shown in Figure 7. Cylindrical dilatometer samples were machined from the mid-thickness of a 215-mm bar of 300 M steel following ASTM A1033.[52] Since the quenching and furnace reheating of a plate using the dilatometer is programmed in linear segments, the nonlinear profiles were segmented to approximate the curvature of the numerically modeled profiles. Segments were chosen to match the desired heating and cooling rates within 0.2 °C/s, and sample temperature matched the desired temperature within 5 °C.

Retained austenite volume fraction measurements were obtained using X-ray diffraction (XRD). XRD was performed using chromium radiation in a Bruker D8 Discover diffractometer equipped with a 1D Linxeye detector. The collimator size was 0.5 mm and operating

Table III. Measured RA Fractions in Q&P, Q&T, and As-Quenched Samples

TP	Q&P		Q&T	
	Measured RA Range (Vol Pct)	Average Carbon Content (Wt Pct)	Measured RA Range (Vol Pct)	Average Carbon Content (Wt Pct)
As-quenched	6 ± 2	0.7 ± 0.2	4.6 to 9.6	0.6 ± 0.1
10,000 (400 °C furnace)	17 ± 4	1.0 ± 0.1	8 ± 1	1.0 ± 0.1
10,000 (500 °C furnace)	15 ± 3	1.0 ± 0.1		
12,000 (400 °C furnace)	18 ± 4	1.2 ± 0.1	7 ± 0	1.1 ± 0.1
12,000 (500 °C furnace)	19 ± 7	1.2 ± 0.1		
8000	7 ± 2	1.0 ± 0.1	7 ± 4	

conditions were 30 kV and 45 mA. Sample preparation was done by sectioning the cylindrical dilatometry samples at the mid-length, between the thermocouple leads. Each half measured 4 to 5 mm in length. Sectioning was done using a low speed saw. One half of each sectioned sample was prepared for XRD; the second half of each sample was used for metallography and hardness testing. One face (the cut face) of each XRD sample was thinned in a solution of 10 parts deionized water, 10 parts hydrogen peroxide, and 5 parts hydrofluoric acid for 5 minutes, to achieve a thickness reduction of at least 0.005 in. as per ASTM standard E975.[53] Each thinned sample was mounted on a zero background diffraction plate, and scanned over a 2θ range of 65 to 165 deg, with a step size of 0.15 deg and a dwell time of 2 seconds. The sample rotated at a speed of 18 deg/min through tilt angles (psi ψ) 0 to 60 deg. Three ferrite/martensite peaks ({110}, {200}, {211},) and three austenite peaks ({111}, {200}, {220},) were analyzed to estimate the amount of RA. Analysis was performed using Rietveld refinement analysis, a pattern matching algorithm. Rietveld analysis was performed using 6 order spherical harmonics to minimize texture effects, and refinement of lattice parameters (both for the BCC and the FCC phases) was permitted. The database used in the analysis was the International Center for Diffraction Data Powder Diffraction File-4, Minerals Database, 2017 (ICDD PDF-4, 2017). The error associated with retained austenite measurement using XRD is estimated to be quite small (a maximum sample standard deviation of 0.05 wt pct).

Carbon contents were estimated according to Eq. [10][54]:

$$a_o = 3.555 + 0.044C\gamma, \qquad [10]$$

where a_o is the austenite lattice parameter in Å and $C\gamma$ is the carbon content of austenite in wt pct.

Vickers microhardness testing of dilatometry samples was performed with a LECO LM110 automatic hardness tester. Samples were polished to a 3-μm finish and tested unetched. A 500-g load was used. All microhardness results are reported as the average of 30 measurements.

V. RESULTS OF LABORATORY SIMULATION OF Q&P PLATE PROCESSING

The process design methodologies developed for the quenching and partitioning steps were assessed by experimental investigation of alloy 300 M. The resulting fractions of retained austenite are given in Table III. RA fractions are reported for each partitioning and tempering condition, as well as in the as-quenched condition. Average carbon content of RA is also given in Table III.

The Q&T and as-quenched microstructures contain similar volumes of RA, as expected. The carbon content of RA in Q&T microstructures increases with tempering, indicating that both tempering and partitioning reactions occurred in the Q&T samples.[55]

The Q&P microstructures contain much larger fractions of retained austenite compared to the Q&T microstructures, indicating that the plate quenching and partitioning process designs were successful in stabilizing substantial amounts of austenite. An example of a Q&P microstructure, containing a mixture of fresh and tempered martensite, in addition to RA, is shown in Figure 8.

The highest RA contents were measured in Q&P samples with TP 10,000 and 12,000. These samples contain similar amounts of RA, although the carbon content is increased in samples with TP 12,000 which have longer furnace residence times compared to TP 10,000. Q&P samples with TP 8000 where partitioning was terminated during the transfer step contained the least RA overall. Additionally, the carbon content of RA was lowest in Q&P samples with TP 8000 (between 0.5 and 1.0 wt pct) and highest for TP 12,000 (between 0.9 and 1.3 wt pct), where furnace residence times were the longest. These results indicate that *effective partitioning of plates can be achieved during furnace reheating*. Furthermore, all furnace parameters selected to achieve TP 10,000 and 12,000 resulted in large volumes of RA; the variation in the furnace ambient temperature (400 °C or 500 °C) and corresponding holding time did not have a clear effect on the RA fraction under equivalent TP conditions. Examination of the simulated furnace partitioning paths shows that the plates reached

slightly different maximum temperatures at equivalent TP under different furnace conditions. For TP 10,000, the maximum plate temperatures were 310 °C and 321 °C for furnace ambient temperatures of 400 °C and 500 °C, respectively. For TP 12,000, the maximum plate temperature achieved in the 400 °C furnace was 394 °C compared to 426 °C in the 500 °C furnace. The TP methodology appears to capture partitioning kinetics sufficiently to suggest equivalent partitioning paths for different furnace reheat parameters. Overall, based on the measured retained austenite amounts in the Q&P and Q&T samples, *the TP methodology was successful in designing effective non-isothermal partitioning treatments for steel plates with elevated Si content*.

The effectiveness of the process models and partitioning treatments might also be assessed by comparing measured and predicted RA fractions. Recall that the quench design methodology predicted the final microstructure based on "ideal" partitioning. "Ideal" phase fractions were calculated for two different assumptions. The first calculation was based on the through-thickness temperature profile at the end of the quench step ("initial QT"). A second calculation represented conditions a few seconds of quenching, after the center and quarter point reached their minimum temperatures (or "final QT"), recognizing the additional cooling that takes place in these locations during equilibration of the through-thickness thermal profile, which may generate some additional martensite after application of the quenchant is completed. The measured RA fractions are compared to the "ideal" phase fractions in Figures 9 through 11 for both quench temperature assumptions. The two conditions are referred to in the caption as the "initial" quench temperatures achieved at the "initial" quench times and the minimum temperature achieved within a few seconds of the end of the quenching step. The figures present the measured phase fractions as a function of position through the plate thickness from center (0 mm) to surface (9 mm), as well as the predicted amounts of retained austenite, martensite, and fresh martensite, assuming ideal partitioning. Figure 9 applies to a quenching time of 15.2 seconds, while Figures 10 and 11 apply to quenching times of 13 and 18.2 seconds, respectively, where the ¼-point temperatures vary by about 50 °C in comparison to Figure 9. The applicable temperatures at the center, surface, and quarter points are indicated on the secondary *x*-axes in Figures 9 through 11 for the two calculations related to martensite transformation during or just after the cooling step, respectively.

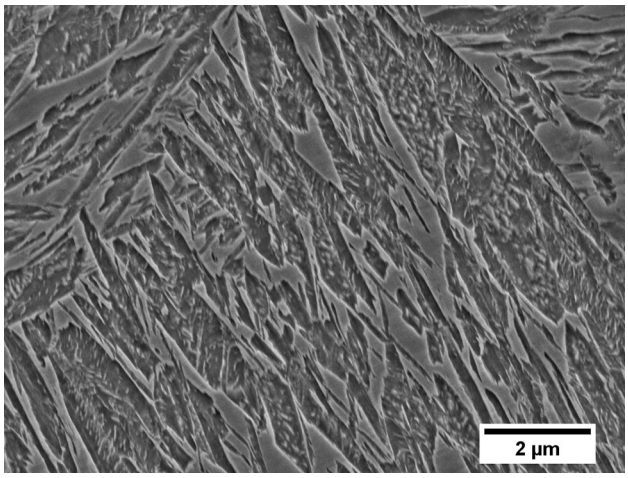

Fig. 8—Secondary electron micrograph of alloy 300 M processed to simulate the center of an 18-mm plate, severe water quenched for 15.2 s, transferred over 5 min and held in a 400 °C furnace for 6 min and 12 s to achieve a TP of 10,000.

The predicted RA fractions based on initial quench temperature are considerably different compared to the fractions predicted based on minimum temperature for initial quench times of 15.2 and 13 seconds. While the predicted results are the same at the surface location, the additional transformation in the subsurface locations (resulting from the additional cooling that occurs after the end of the cooling step) leads to a reduction in the amount of fresh martensite in these locations, as well as a change in the retained austenite profile. These differences in predicted phase fraction are less pronounced in

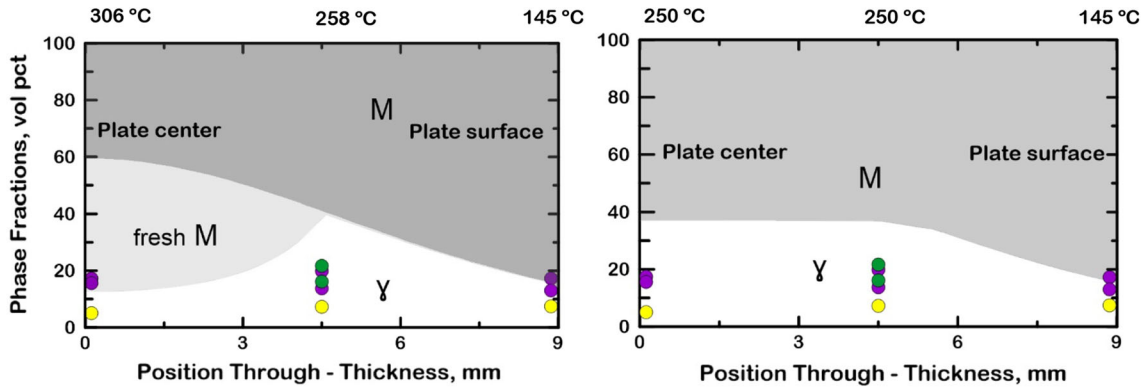

Fig. 9—Estimated final phase fractions (assuming full partitioning) of 300 M as a function of position through the plate thickness from center to surface for an initial quench time of 15.2 s. Estimated phase fractions are shown based on initial quench temperature (left) and minimum temperature achieved at each location within a few seconds of quenching (right). The measured RA phase fraction is shown for all experimental partitioning conditions, with partitioning parameters of 8000 (yellow), 10,000 (purple), and 12,000 (green). Plate temperatures used to estimate phase fractions at the center, surface, and quarter point are indicated on the secondary *x*-axis (Color figure online).

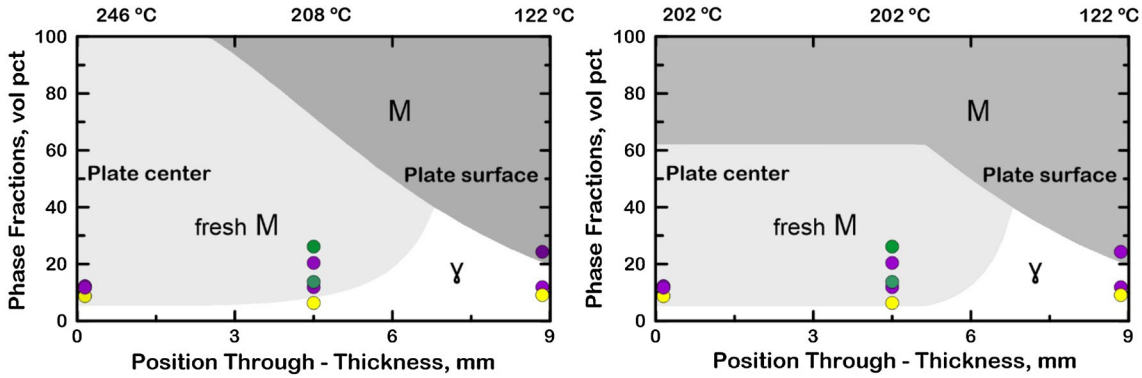

Fig. 10—Estimated final phase fractions (assuming full partitioning) of 300 M as a function of position through the plate thickness from center to surface for an initial quench time of 13 s. Estimated phase fractions are shown based on initial quench temperature (left) and minimum temperature achieved at each location within a few seconds of quenching (right). The measured RA phase fraction shown for all experimental partitioning conditions, with partitioning parameters of 8000 (yellow), 10,000 (purple), and 12,000 (green). Plate temperatures used to estimate phase fractions at the center, surface, and quarter point are indicated on the secondary *x*-axis (Color figure online).

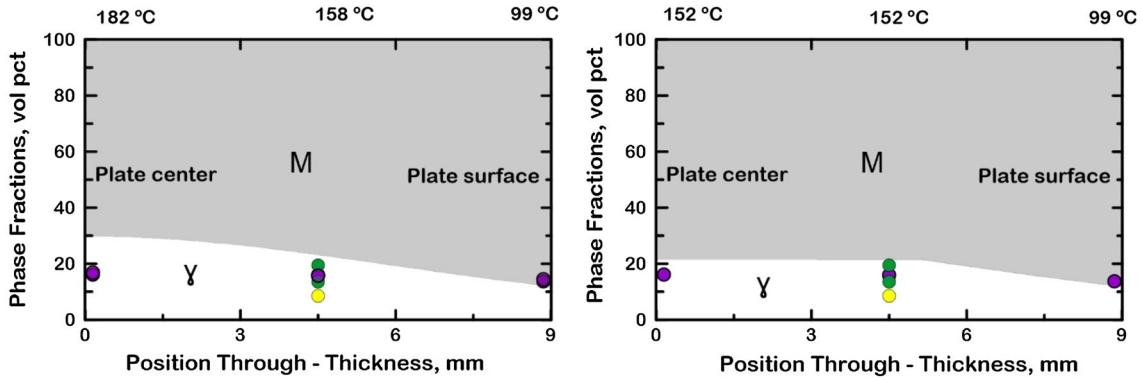

Fig. 11—Estimated final phase fractions (assuming full partitioning) of 300 M as a function of position through the plate thickness from center to surface for an initial quench time of 18.2 s. Estimated phase fractions are shown based on initial quench temperature (left) and minimum temperature achieved at each location within a few seconds of quenching (right). The measured RA phase fraction shown for all experimental partitioning conditions, with partitioning parameters of 8000 (yellow), 10,000 (purple), and 12,000 (green). Plate temperatures used to estimate phase fractions at the center, surface, and quarter point are indicated on the secondary *x*-axis (Color figure online).

Figure 11 that applies to the 18.2 initial quench time, because, for this longer quenching step, plate cooling has progressed to lower temperatures (below the ''optimum'' quench temperature at all locations) where fresh martensite is no longer expected after ideal partitioning.

The *measured* retained austenite profiles in the experimentally quenched and partitioned specimens do not closely match either set of predictions. For an initial quench time of 15.2 seconds, a maximum of 38 vol pct retained austenite is predicted for this condition that corresponds to the ''optimum'' QT at the quarter point (and in the center when additional cooling during equilibration is considered). While the maximum amount of retained austenite was measured at the 1/4-thickness location for this simulated quench time, the amount was about 22 vol pct.

For an initial quench time of 13 seconds (Figure 10), the measured austenite profile through the thickness again exhibited less variation than expected (in comparison to the calculated profiles). Interestingly, the measured austenite fraction exceeded the calculated amounts in several instances, particularly at the subsurface locations. For an initial quench time of 18.2 seconds, the fraction of retained austenite was not expected to vary much with position through the thickness (Figure 11). The experimental results are somewhat consistent with the shape of the predicted austenite profile, although the measured retained austenite fractions are still less than calculated assuming idealized partitioning.

Since the measured fractions do not closely match the predicted amounts, it is clear that the relationship between the temperature achieved during quenching and the final RA is not yet fully understood. Nonetheless, appreciable amounts of austenite were retained at all simulated through-thickness locations for all three quench times, verifying the effectiveness of plate Q&P processing. The sensitivity of measured RA content to QT was also less than anticipated. Less sensitivity of RA to QT than predicted has been reported previously in other Q&P studies,[17,18,56] particularly when incorporating partitioning kinetics[18,27,57] although the range of examined QT was narrower in these earlier studies. This behavior, including the role of kinetics, would be

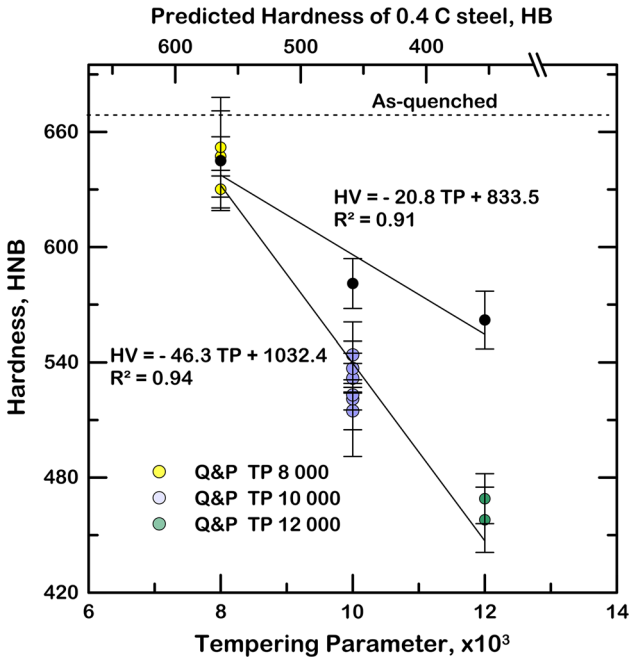

Fig. 12—Brinell hardness measurements for Q&T samples and quarter point Q&P samples plotted as a function of tempering parameter. The predicted hardness of a 0.4 wt pct carbon C Q&T steel is shown on the secondary *x*-axis for each tempering parameter. The as-quenched martensite hardness is indicated with the dashed horizontal line.

worthwhile to confirm over a greater range of alloys and quench temperatures in Q&P plate processing, since insensitivity to processing variations might be considered a desirable attribute in industrial processing. For example, insensitivity to QT would reduce the through-thickness microstructure gradients, and also allow for more flexibility to produce thicker Q&P plates (thicker plates are associated with greater thermal and microstructure gradients). Furthermore, the initial quench time may not have to be as tightly controlled to produce Q&P microstructures successfully. Factors that contribute to discrepancies in predicting the Q&P microstructure include (1) optimized partitioning treatments are less than "ideal," due to other mechanisms that compete with partitioning, (2) the M_s temperature and progress of martensite transformation with undercooling are not represented sufficiently by the empirical relationships employed, and (3) the degree of autotempering or "autopartitioning" that occurs during cooling at different plate positions, and their influence on the local martensite transformation behavior during later cooling to room temperature.[11]

In addition to predictions and measurement of austenite phase fractions, the hardness of the final microstructure was also predicted and measured. The hardness of all Q&P samples was measured for the quarter point simulations, and can be compared with the Q&T sample hardness at equivalent TP values in Figure 12. For reference, the figure also shows the predicted hardness for a conventionally quench and tempered "generic" 0.42 wt pct C steel. Over the range of TP examined, the measured hardness of both Q&T and Q&P 300 M is greater than predicted for a 0.4 C steel, with increasing disparity at higher TP. This behavior is perhaps not surprising for 300 M, which is known to exhibit tempering resistance due to its elevated silicon addition.

Comparing the softening behavior of the Q&P and Q&T microstructures in Figure 12 provides some insight into the mechanisms active during the tempering and partitioning treatments. The softening behavior of both (quarter point) Q&P and Q&T microstructures is approximately linear with respect to TP between 8000 and 10,000, although, over a wider range of TP, the softening behavior of 300 M would not be expected to exhibit linearity.[58] Between TP 8000 and 10,000, both Q&P and Q&T microstructures softened with increasing TP, though at different rates. At a TP of 8000, both Q&T and Q&P microstructures had similar hardnesses, but at higher TP the Q&T microstructures resisted softening more than the Q&P microstructures. As the hardness of martensite is related to its carbon content,[51] it is speculated that carbon partitioning from martensite to austenite occurs on a shorter timescale[1,10,59] than reactions associated with tempering, including precipitation of carbides.[40] The softening behavior shown in Figure 12 may indicate that partitioning occurred in the Q&P samples, while tempering reactions were dominant in the Q&T samples. While silicon is usually considered in terms of its influence on austenite retention in Q&P steels, the hardness behavior in this work perhaps also illustrates a contribution of silicon to the strength of Q&P steels, both through solid solution strengthening and through its influence on tempering resistance (*e.g.,* cementite formation) of the martensite matrix.

VI. CONCLUSIONS

Methodologies have been developed for the design of quenching and partitioning treatments to produce Q&P plate steel. The design methodologies assist in the selection of key processing parameters. The quenching step methodology is based on the "optimum" QT, and the partitioning methodology is based on the Hollomon–Jaffe tempering parameter, applied here for partitioning in a furnace after plate quenching.

Experimental verification of the process designs was undertaken by laboratory simulation of Q&P plate processing using alloy 300 M. The physical simulations produced microstructures containing amounts of RA between 5 and 27 vol pct at the center, surface, and quarter point of an 18-mm plate. The presence of substantial austenite fractions verified that the tempering parameter methodology was successful in the design of furnace partitioning treatments. Thermal histories associated with tempering parameter values of TP 10,000 and 12,000 provided highly successful partitioning treatments. The furnace ambient temperature for equivalent TP did not appear to influence the final RA fraction.

The volume fraction of RA was found to be less sensitive to initial quench temperature than predicted by the quench step design methodology involving ideal partitioning. Nonetheless, appreciable amounts of austenite were retained through the simulated plate thickness regardless of initial quench time. This insensitivity to quenching conditions indicates that additional fundamental studies are needed to better understand the microstructure development, but may suggest behavior that would be considered beneficial in the context of robust industrial implementation.

Most importantly, the combined modeling and experimental work confirmed the viability of plate Q&P processing and verified the utility of furnace reheating as a viable partitioning process.

ACKNOWLEDGMENTS

The sponsors of the Advanced Steel Processing and Products Research Center at Colorado School of Mines are gratefully acknowledged. Dr. E.B. Damm and Timken Steel are gratefully acknowledged for providing the experimental steel. Ana Araujo and AK Steel are gratefully acknowledged for contributions to the characterization portion of this work, including XRD and SEM.

REFERENCES

1. A.J. Clarke, J.G. Speer, M.K. Miller, R.E. Hackenberg, D.V. Edmonds, D.K. Matlock, F.C. Rizzo, K.D. Clarke, and E. De Moor: *Acta Mater*., 2008, vol. 56, pp. 16–22.
2. D.K. Matlock and J.G. Speer: *Mater. Manuf. Process*., 2010, vol. 25, pp. 7–13.
3. L. Wang and W. Feng: *Advanced Steels: The Recent Scenario in Steel Science and Technology*, W. Yuqing, H. Dong, and G. Yong, eds., Springer, Berlin, 2011, pp. 67–73.
4. T. Liu, M.T. Kiser, and T.E. Clements: *Proceedings of 2011 International Symposium on the Recent Developments in Plate Steels, AIST*, 2011, pp. 71–80.
5. R. Youngblood: M.S. thesis, Colorado School of Mines, Golden, CO, 2018.
6. S.W. Lee and H.C. Lee: *Metall. Trans*., 1993, vol. 24, pp. 1333–43.
7. S.C. Hong, C.J. Ahn, S.Y. Nam, S.J. Kim, C.H. Yang, J.G. Speer, and D.K. Matlock: *Met. Mater. Int*., 2007, vol. 13, pp. 439–45.
8. B.C. De Cooman and J.G. Speer: *Fundamentals of Steel Product Physical Metallurgy*, ASM International, Warrendale, 2011.
9. J. Speer, D.K. Matlock, B.C. De Cooman, and J.G. Schroth: *Acta Mater*., 2003, vol. 51, pp. 2611–22.
10. D.K. Matlock, V.E. Brautigam, and J.G. Speer: *Mater. Sci. Forum*, 2003, vols. 426–4, pp. 1089–94.
11. A.J. Clarke, J.G. Speer, D.K. Matlock, F.C. Rizzo, D.V. Edmonds, and K. He: *Miner. Met. Mater. Soc*., 2003, vols. 172–174, pp. 99–108.
12. D.B. Futch, G.A. Thomas, J.G. Speer, and K.O. Findley: *Iron Steel Technol*., 2012, vol. 2012, pp. 101–06.
13. J.G. Speer, A.L. Araujo, K. Matlock, E. De Moor, and J. Speer: *Mater. Sci. Forum*, 2017, vol. 879, pp. 1834–40.
14. M.J. Kähkönen, E. De Moor, J.G. Speer, and G. Thomas: *SAE Int. J. Mater. Manuf*., 2003, vol. 8, pp. 419–24.
15. M.J. Santofimia, L. Zhao, R. Petrov, C. Kwakernaak, W.G. Sloof, and J. Sietsma: *Acta Mater*., 2011, vol. 59, pp. 6059–68.
16. D. De Knijf, E.P. Da Silva, C. Föjer, and R. Petrov: *Proc. Mater. Sci. Technol*., 2015, vol. 31, pp. 817–28.
17. J.G. Speer, E. De Moor, A.J. Clarke, and E. De Moor: *Proc. Mater. Sci. Technol*., 2015, vol. 31, pp. 3–9.
18. A.J. Clarke, J.G. Speer, D.K. Matlock, F.C. Rizzo, D.V. Edmonds, and M.J. Santofimia: *Scripta Mater*., 2009, vol. 61, pp. 149–52.
19. W. Wang, H. Wang, S. Liu, and A. Yang: *Proceedings of Pacific Rim International Conference on Advanced Materials and Processing* (*PRICM9*), 2016, pp. 108–13.
20. G.A. Thomas, J.G. Speer, and D.K. Matlock: *International Conference on New Developments in Advanced High-Strength Sheet Steels, AIST*, 2008, pp. 227–36.
21. X.D. Wang, Z.H. Guo, and Y.H. Rong: *Mater. Sci. Eng., A*, 2011, vol. 529, pp. 35–40.
22. T.Y. Hsu and Z. Xu: *Proceedings of Pacific Rim International Conference on Advanced Materials and Processing* (*PRICM6*), 2007, pp. 2283–86.
23. H. Liu, X. Lu, X. Jin, H. Dong, and J. Shi: *Scripta Mater*., 2011, vol. 64, pp. 749–52.
24. S. Zhou, K. Zhang, N. Chen, J. Gu, and Y. Rong: *ISIJ Int*., 2011, vol. 51, pp. 1688–95.
25. M.C. Somani, L.P. Karjalainen, D.A. Porter, and D.K. Misra: *Mater. Sci. Forum*, 2012, vols. 706–709, pp. 2824–29.
26. M.C. Somani, J.I. Hannula, A.J. Kaijalainen, D.K. Misra, and D.A. Porter: *Proceedings of THERMEC*, 2016, pp. 1819–27.
27. A.J. Clarke: Ph.D. thesis, Colorado School of Mines, Golden, CO, 2006.
28. M.C. Somani, D.A. Porter, P.K. Karjalainen, and M.K. Devesh: *Int. J. Metall. Eng*., 2013, vol. 2, pp. 154–60.
29. R.A. Stewart, J.G. Speer, B.G. Thomas, A.J. Clarke, and E. De Moor: *Iron Steel Technol*, 2017, vol. 2017, pp. 78–87.
30. C.R. Brooks: *Principles of the Heat Treatment of Plain Carbon and Low Alloy Steels*, ASM International, Materials Park, 1996.
31. G.E. Totten and M.A.H. Howes: *Steel Heat Treatment Handbook*, G.E. Totten and M.A.H. Howes, eds., Marcel Dekker, Inc., New York, 1997, pp. 185–97, 210–47.
32. T.L. Bergman and A.S. Lavine: *Fundamentals of Heat and Mass Transfer*, 7th ed., Wiley, Hobokon, 2011.
33. C. Li and B.G. Thomas: *Metall. Mater. Trans. B*, 2004, vol. 35B, pp. 1151–72.
34. H. Sadiq, M.B. Wong, J. Tashan, R. Al-Mahaidi, and X.L. Zhao: *J. Mater. Civ. Eng*., 2013, vol. 25, pp. 167–73.
35. K. Okamoto, A. Yoshie, and H. Nakao: *Physical Metallurgy of Direct-Quenched Steels, Proceedings of TMS*, 1992.
36. Y. Meng and B.G. Thomas: *Metall. Mater. Trans. B*, 2006, vol. 34, pp. 685–705.
37. G.E. Totten and M.A.H. Howes: *Steel Heat Treatment*, 1st ed., Marcel Dekker Inc., New York, 1997.
38. G. Thomas: M.S. thesis, Colorado School of Mines, Golden CO, 2009.
39. J.H. Hollomon and L.D. Jaffe: *Transactions of AIME*, 1945, vol. 162, pp. 223–49.
40. G. Krauss: *Steels Processing, Structure and Performance*, ASM International, Materials Park, 2005.
41. R.A. Grange, C.R. Hribal, and L.F. Porter: *Metall. Trans. A*, 1977, vol. 8A, pp. 1775–85.
42. J. Kahkonen: M.S. thesis, Colorado School of Mines, Golden, CO, 2016.
43. A.L. Araújo: M.S. thesis, Colorado School of Mines, Golden, CO, 2016.
44. C. Hensley: M.S. thesis, Colorado School of Mines, Golden, CO, 2016.
45. X.D. Tan, X.L. Yang, Y.B. Xu, Z.P. Hu, F. Peng, H. Zhang, Y.M. Yu, and D. Wu: *Mater. Sci. Forum*, 2015, vol. 816, pp. 736–42.
46. F.L.H. Gerdemann, J.G. Speer, and D.K. Matlock: *Proceedings of MS&T*, 2004, pp. 439–49.
47. A. Shutts: M.S. thesis, Colorado School of Mines, Golden, CO, 2006.
48. S. Yan and X. Liu: *Adv. Mater. Res*., 2015, vol. 1082, pp. 202–07.
49. Y. Xu, X. Tan, X. Yang, Z. Hu, F. Peng, D. Wu, and G. Wang: *Mater. Sci. Eng., A*, 2014, vol. 607, pp. 149–60.
50. T. Ohtani and H. Kunitake: *Sumitomo Search*, 1969, vol. 2, pp. 18–21.
51. G. Krauss: *Steels Processing, Structure, and Performance*, Materials Park, ASM International, 2005, pp. 297–300.

52. ASTM E975-13: *Standard Practice for Quantitative Measurement and Reporting of Hypoeutectoid Carbon and Low-Alloy Steel Phase Transformations*, ASTM International, Materials Park, 2015.
53. ASTM E975-13: *Standard Practice for X-ray Determination of Retained Austenite in Steel with Near Random Crystallographic Orientation 1*, ASTM International, Materials Park, 2013.
54. B.D. Cullity and S.R. Stock: *Elements of X-ray Diffraction*, 3rd ed., Prentice Hall, Upper Saddle River, 2001.
55. E. De Moor, C. Föjer, J. Penning, A.J. Clarke, and J.G. Speer: *Phys. Rev. B*, 2010, vol. 82, pp. 104210-1–5.
56. G.A. Thomas: Ph.D. thesis, Colorado School of Mines, Golden, CO, 2012.
57. M.J. Santofimia, J.G. Speer, A.J. Clarke, L. Zhao, and J. Sietsma: *Acta Mater.*, 2009, vol. 57, pp. 4548–57.
58. R. Steiner: *ASM Handbook. Properties and Selection: Irons, Steels, and High-Performance Alloys*, 10th ed., ASM International, Materials Park, 1990, vol. 1.
59. F. Gerdemann: M.S. thesis, Colorado School of Mines, Golden, CO, 2004.